SECED 2023 Conference
Earthquake Engineering & Dynamics for a Sustainable Future
14-15 September 2023, Cambridge, UK

ESTIMATING THE YIELDING DISPLACEMENT AND SHEAR DEMAND OF A SLENDER CANTILEVER REINFORCED CONCRETE WALL INCLUDING SYSTEM AND CYCLIC EFFECTS

Patricio QUINTANA GALLO[1] & Farhad DASHTI[2]

Abstract: *In some current seismic code provisions and design philosophies/methodologies, the plastic hinge method is used for relating the lateral top-displacement (Δ) of cantilever reinforced concrete walls to the curvature, and, assuming plain-sections, to the strain demand developed in their critical cross-section. Using specified values of the ultimate strains assigned to concrete and steel (e.g. crushing, buckling), the ultimate inelastic top-displacement capacity of the wall (Δ_u) is found. The computation of Δ_u requires the estimation of the yielding top-displacement (Δ_y). Classically, to compute Δ_y and hence Δ_u, it is assumed that a lateral load imposes a first-mode deflected shape of the wall and the yielding curvature is reached at its critical cross-section, assuming that the same load pattern, and, therefore, the same moment-to-shear ratio of the base reactions, equal to the effective height (h) of the lateral external load, is the same for all the walls part of a structure. In 2022, using a refined finite element model (FEM) and pushover analyses, the authors showed that this assumption is incorrect for a system of walls of different cross-section lengths having rigid diaphragm lateral displacement compatibility at each storey level, and used the term 'system effect'. They also proposed a novel formula for computing Δ_y as a function of h obtained for each wall with a linear-elastic analysis of the system under a reference external loading. It was shown that the estimated values of Δ_y were in good agreement with the FEM results, but the classic ways were sometimes far unconservative, posing a warning flag for the adequacy of current design practice. This paper presents a concise summary of the findings of such an investigation and addresses the same problem but including cyclic quasi-static external loading to investigate how it affects the results previously found under monotonic loading.*

Introduction

It appears safe to say that the large majority of reinforced concrete (RC) buildings is structured with walls of different cross-section lengths. In most of the cases, stiff, long, highly resistant walls are combined with more flexible, less strong, shorter walls. The relevance of a wall cross-section length (l_w) on its base shear-top displacement (V_0-Δ) response is at least twofold, such that the greater the value of l_w: (1) the larger the flexural strength and the lateral stiffness (for the same amount of vertical reinforcement); and (2) the smaller the cross-section yielding curvature (ϕ_y), because $\phi_y = \eta\varepsilon_y/l_w$, where ε_y is the yielding strain of the reinforcing steel, and η normally takes values between 1.5 and 2.0 for rectangular walls.

To design each of the walls forming a structure (building), it is common practice to assume that they are independent from the rest of the structure. That is to say, the effect of the stiffer walls over the shorter ones, and vice versa, is not considered, even if they are, in multi-storey buildings, almost always interconnect by means of floor slabs at each storey level, or at least at some of them. For instance, for a given lateral load, if no capacity design considerations, in the sense of Paulay and Priestley (1992), are included, V_0 affecting each of the walls would simply be proportional to either their flexural strength (e.g. $V_0 = M_n/h_w$ for a limit analysis with lumped lateral load at the top; M_n is the nominal moment at the base) or to I_w^3, per a linear elastic analysis.

In addition, Δ producing yielding at the base of a wall, Δ_y, is classically computed under the aforementioned independence assumption, such that $\Delta_y = \gamma\phi_y h_w^2$, where h_w is the height of the wall, and γ is a constant that depends on the presupposed deflected shape of the wall imposed by a given lateral load pattern (γ = 1/3 (Paulay & Priestley 1993); γ = 11/40 (Wallace & Moehle

[1] Postdoctoral Fellow, Czech Technical University in Prague, Prague, Czech Republic, patricio.gallo@fsv.cvut.cz
[2] Research Director - Structural/Earthquake Engineering, ZURU Tech HK Ltd, Tsim Sha Tsui, Hong Kong

1992). Consequently, for walls of the same height, Δ_y of very short walls would be estimated to be much larger than those of very long and stiff walls, because it holds that $\Delta_y = \gamma\eta\varepsilon_y h_w^2/l_w$.

Nevertheless, based on numerical results, different researchers (e.g. Rutenberg (2004) and Beyer et al. (2014)) have shown that the base shear taken by the shorter walls would be much larger than anticipated under the independence assumption if they are treated as interconnected members having lateral displacement compatibility at each storey level (diaphragm action). More recently, Quintana Gallo et al. (2022) focused on showing that not only V_0 of the shorter walls within a system of four walls of different lengths is greater than if treated independently, but also the yielding displacement and the maximum displacement capacity would be affected. That is to say, considering the numerical results obtained with a refined finite element model constructed in the software DIANA (DIANA 2017), it was concluded that the shorter walls would have: (a) larger V_0, (b) smaller Δ_y; and (c) smaller Δ_u, when analysed within the whole system compared to as analysed independently (named "system effect").

Building on the latter research, the present paper evaluates the differences in V_0 and Δ_y found with numerical analyses due to system effects but using cyclic instead of monotonic loading. The hysteresis V_0-Δ curves obtained for each of the four walls of the case-study example, treated as a system and independently, are presented, showing that relevant differences arise between the response of the walls in both cases. The hysteresis loops are also compared with the corresponding monotonic curves, depicting that the latter approximately match the positive backbone curves of the cyclic responses, but do not always match the negative ones, due to the existence of static shear forces.

System effect: conceptualization and analytical formulation

Past research has shown, using numerical methods, that the response of cantilever RC walls is not the same if they are analysed separately or interconnectedly (system effect). In particular, Quintana Gallo et al. (2022) proposed a physically meaningful analytical way of addressing this effect, with the intention of providing a tool for practical design with a robust theoretical background. The method uses the concept of a reduced effective height of the equivalent lateral force (V_0) of a wall, $h = M_0/V_0$, referred to that found for a shape representative of the first mode (typical case). This is equivalent to the way dynamic effects are included in the calculation of the capacity-based shear demand for walls (Paulay 1983; Paulay & Priestley 1992), and in the calculation of Δ_y, as more recently proposed by Quintana Gallo (2018), where γ is a function of h.

Fig. 1a shows a system of two walls, with different cross-section lengths, $l_{w,1}$ and $l_{w,2}$, subjected to an inverted triangle distributed lateral load. This figure also shows the equivalent external load applied to the system and its effective height, named V_0^S and h^S, respectively, where the superscript S refers to 'system'. Fig. 1b presents one of the two walls forming the system shown in Fig. 1a, generically referred to as wall 'i', subjected to the same load acting over the system, such that $h_i^I = h^S$ ('I' refers to 'independent'). Fig. 1c, shows wall i presented in Fig. 1b, resisting the lateral load $V_{0,i}^S$ acting at a reduced (or increased) height compared to h^S, and referred to as h_i^S. As shown in Fig. 1c, the effective heights of both cases, are related to each other by the so-called "system factor": $\lambda_{S,i} = h_i^S/h_i^I = h_i^S/h^S$, with $\lambda_{S,i} > 0$. For the same resisting moment at the base of the wall i in the independent and system cases ($M_{0,i}^I = M_{0,i}^S$), the base shear demand over wall i, accounting for the system effect is $V_{0,i}^S = \lambda_{S,i} V_{0,i}^I$. The effective heights shown in Fig. 1 are divided by the height of the wall, h_w, and the following dimensionless terms are defined: $\alpha_i = h_i^I/h_w$, and $\alpha_{S,i} = h_i^S/h_w$, with $\alpha_{S,i} = \alpha_i/\lambda_{S,i}$.

The proposed analytical expression (developed for a cantilever wall) assumes that: (a) the wall is slender; (b) the inelasticity occurs at the base of the wall only; (c) the cross-sectional stiffness (EI) is the same along the entire height of the wall and equal to that of the cross-section at the base; (d) the moment-curvature relationship at the base of the wall is described by a tri-linear curve (Fig. 2a); and (e) beyond the yielding point, the wall pivots as a rigid body about a point located $l_p/2$ above the base, as in the classical plastic hinge method (l_p is the plastic hinge length).

The top lateral displacement, Δ, is computed as that resulting from the action of a lateral force V_0 acting at the effective height $\alpha_S h_w$. The cracking and yielding displacements, Δ_{cr}^S and Δ_y^{Sm}, are given by Eq. (1) and Eq. (2), respectively (ϕ_{cr} is the cracking curvature). Note that the preliminary yielding displacement, named Δ_y^S, is modified by a factor λ_y which may account for differences in the value of EI along the height of the wall. The full analytical expression of the V_0-Δ pushover curve is presented in Eq. (3). This expression is depicted in Fig. 2b, where EI_g is the gross cross-

section stiffness, q and s are the post-cracking and post-yielding cross-section stiffness factors, respectively, and $\psi = l_p/h_w$. It is important to note that EI_g should be the gross section of the transformed section to concrete, i.e. including the additional stiffness provided by the steel bars. In some cases, as in this example, because the amount of vertical steel is relatively low, the effect of the steel can be neglected, but in largely reinforced very short walls it may be non-negligible.

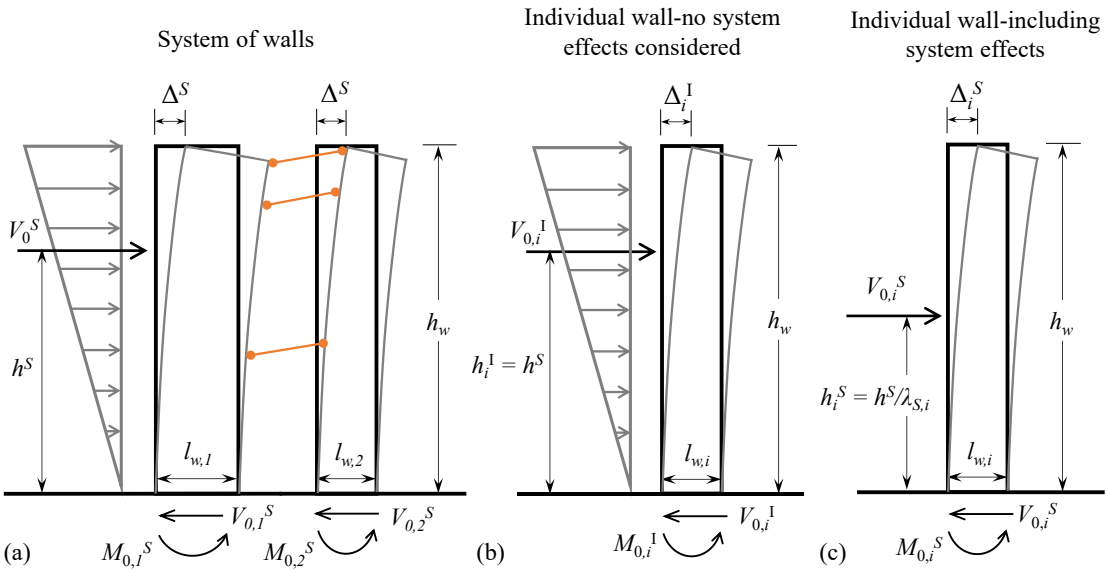

Figure 1. Accounting for "system effect" in the analysis of independent walls: a system of walls; b individual wall no system effects considered; c individual wall system effects considered (reprinted from Quintana Gallo et al. (2022) with permission from Springer Nature)

$$\Delta_{cr} = \frac{\alpha_S}{6}\left(3-\alpha_S\right)\phi_{cr}h_w^2 \tag{1}$$

$$\Delta_y^{Sm} = \lambda_y \frac{\alpha_S}{6}\left(3-\alpha_S\right)\phi_y h_w^2 \tag{2}$$

$$V_0 = \begin{cases} \left(\dfrac{EI_g}{h_w^3}\right)\dfrac{6}{\alpha_S^2\left(3-\alpha_S\right)}\Delta & \text{for } 0 \le \Delta \le \Delta_{cr}^S \\ \left(\dfrac{qEI_g}{h_w^3}\right)\left[\dfrac{\phi_{cr}h_w^2}{\alpha_S q} + \dfrac{6}{\alpha_S^2\left(3-\alpha_S\right)}\dfrac{\left(\phi_y-\phi_{cr}\right)}{\left(\lambda_y\phi_y-\phi_{cr}\right)}\left(\Delta-\Delta_{cr}\right)\right] & \text{for } \Delta_{cr}^S \le \Delta \le \Delta_y^{Sm} \\ \left(\dfrac{sEI_g}{h_w}\right)\left(\dfrac{1}{\alpha_S s}\left[\phi_{cr}+q\left(\phi_y-\phi_{cr}\right)\right]+\dfrac{\left(\Delta-\Delta_y\right)}{\alpha_S h_w^2\left(\psi-\psi^2/2\right)}\right) & \text{for } \Delta_y^{Sm} \le \Delta \le \Delta_u^S \end{cases} \tag{3}$$

The parameter α_S is found with a simple linear elastic analysis of the system of walls (using their gross cross-sectional properties), subjected to the specified external loading. This is consistent with the approach proposed by Paulay (1983) and Paulay & Priestley (1992) for capacity-based design for shear. The ultimate displacement, Δ_u^S, is found with the expression $\Delta_u^S = \Delta_y^{Sm} + (\psi - \psi^2/2)(\phi_u - \phi_y)h_w^2$, which corresponds to that obtained with the plastic hinge method.

It is very important to note that in Quintana Gallo et al. (2022), the factor λ_y was introduced to reduce the yielding displacement obtained without considering it, given by $\Delta_y^S = (\alpha_S/6)(3 - \alpha_S)\phi_y h_w^2$. It is written in that paper that even though the yielding lateral force was computed with Δ_y^S, the yielding displacement is computed as $\Delta_y^{Sm} = \lambda_y\Delta_y^S$, i.e., with Equation (2). It was proposed to take $\lambda_y = 0.6$ for the case under investigation as it suited all of the four cases. However, quite regretfully, there was an error in the plotting of the displacement of the walls for the FEM case. That is to say, the lateral displacement was not that of the top of the walls, but the one computed at $0.7h_w$, where the displacement was actually imposed. An errata request is being sent to the journal at the time of writing.

On the flip side, though, after using the correct lateral displacement values obtained with FEM, the formulation does not require the ad-hoc modification factor λ_y, such that the analytical procedure is more robust and does not need to be 'patched' (in the sense of Karl Popper) with λ_y. The consequence is a higher scientific status of the formulation. Nevertheless, as with some mistakes, possibilities for improvement can be opened, so that λ_y is kept in the general formulation presented in Eq. (1) to (3) but set to λ_y = 1.0 for the case under examination. This value could change, nonetheless, for different values of h_w, for instance. Alternatively, λ_y can be thought of as a reduction factor of ϕ_y, for example. In the following, the analytical prediction is computed with λ_y = 1.0 in all of the cases, whereas the correct values of the top-displacements are used.

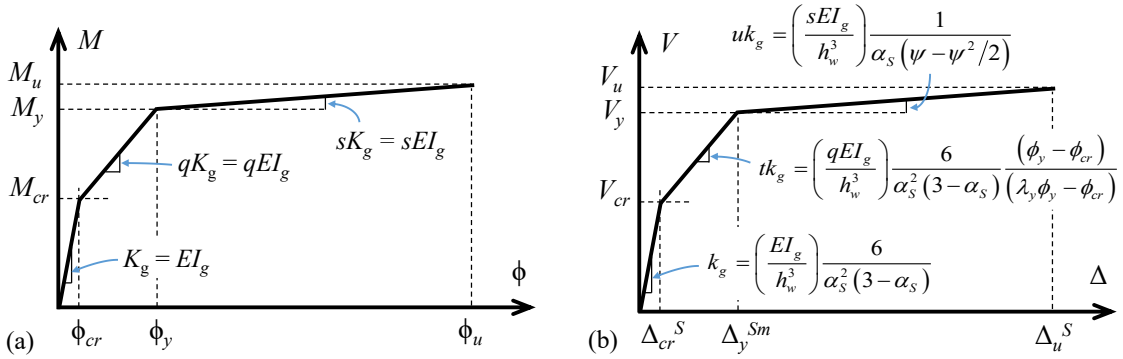

Figure 2. V_0-Δ piecewise-linear formulation for individual walls accounting for system effects: a moment-curvature relationship at the base of the walls; b proposed base shear vs top-displacement envelope (reproduced from Quintana Gallo et al. (2022) with permission from Springer Nature).

Case-study description

Fig. 3 presents the floor layout of all the 10 storeys of the case-study structure considered in this work. 150 mm thick cast-in-situ slabs are assumed to impose a rigid diaphragm action at each storey level. The seismic weight (computed as the dead load plus 25% of the live load) and the height of the structure are W_s = 7070 kN and H_t = 25.0 m, respectively. The geometry of the four types of walls forming the structure is summarized in Table 1, which also provides, for each wall: (a) the axial load P; (b) $u = P/f_c'A_g$; (c) the distributed web-rebar (vertical and horizontal); (d) the amount of longitudinal and transverse reinforcement at the ends; (e) the length of the confinement elements (Fig. 3). The following material properties were assumed: concrete with compression strength f_c' = 30 MPa; and steel grade Gr.60 (f_y = 420 MPa and f_u = 630 MPa).

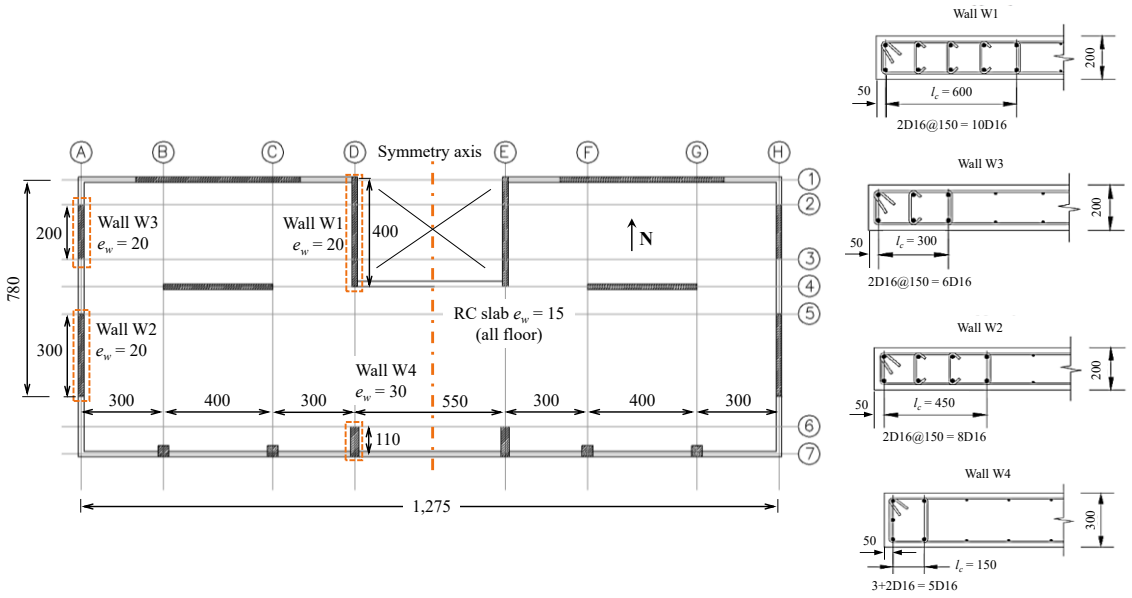

Figure 3. Case-study description: floors layout and wall detailing: (a) W1; (b) W2; (c) W3; and (d) W4 (reproduced from Quintana Gallo et al. (2022) with permission from Springer Nature).

Wall ID	l_w (cm)	A_r	e_w (cm)	P (kN)	v = P/f_c'A_g	Distributed Vertical & Horizontal Rebar	End vertical rebar	Confinement boundary elements	Confined length (cm)
W1	400	6.25	20	2350	0.098	2D8@200	10D16	D8@100	60
W2	300	8.33	20	1890	0.105	2D8@200	8D16	D8@100	45
W3	200	12.50	20	900	0.075	2D8@200	6D16	D8@100	30
W4	110	22.73	30	1930	0.195	2D8@200	5D16	D8@100	15

Table 1. Walls dimensions, reinforcement, and other properties.

Summary of previous results obtained with pushover analyses

The case-study structure, formerly designed by Alvarez (2019), was analysed in the N-S direction under monotonic loading (pushover). The seismic-resistant system of the building in such a direction was idealized, making use of symmetry, as a system of the four walls identified in Fig. 3 (named W1 to W4). For the system case, the floor slabs were assumed to be able to impose lateral displacement compatibility at each storey level (i.e., diaphragm effect), but had no flexural resistance/stiffness. The system was modelled using lumped-inelasticity macro-elements with a piecewise-linear skeleton (bi-linear and tri-linear); a strut-and-tie model (SAT); and a finite element model (FEM) constructed in DIANA (2017) (see Dashti et al. (2017)).

The numerical results obtained with FEM showed significant differences between the monitored parameters of the response of some of the walls for the independent and system cases. Overall, Δ_y of the shorter walls W2, W3, and W4, decreased, whereas for the longest wall (W1) this parameter slightly increased; and the maximum shear force, V_0^{max}, of the shortest walls (W3 and W4) significantly increased, while that of the others did not change or slightly decreased.

For wall W4, the results showed discrepancies of approximately half and four times for Δ_y and V_0^{max}, respectively (Fig. 4). The numerical results showed that h remained constant and equal to $0.7h_w$ for the independent cases, whereas it varied significantly for all the walls when interconnected (Fig. 4). However, h obtained from an elastic analysis of the system may be used as a conservative lower bound, as shown in Fig. 4. This is exactly the same approach as the one proposed by Paulay (1983) for capacity-based design for shear. In this case, α_S was 0.9, 0.65, 0.45, and 0.30 for walls W1 to W4, respectively. Using these values, the proposed analytical formulation provided a conservative and accurate estimation of the V_0-Δ curves of each wall including system effects, as shown in the following.

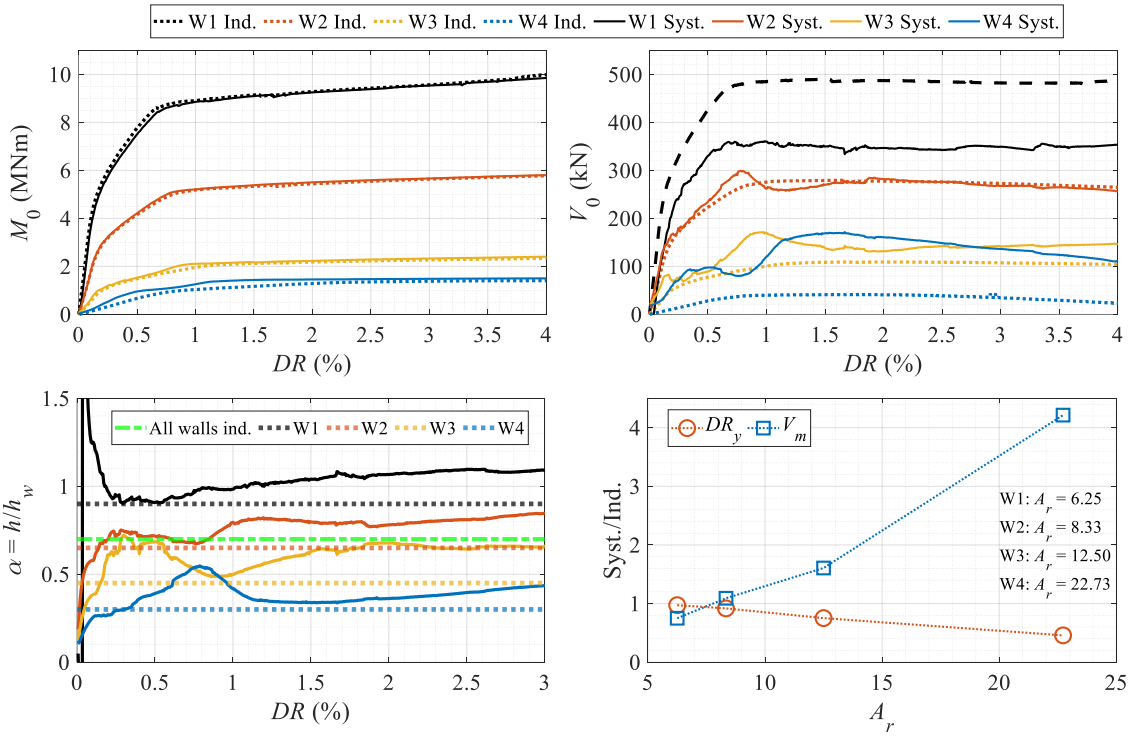

Figure 4. Summary of previous results obtained with pushover analyses for V_0^{max}, h_i^S, and Δ_y

Results of cyclic quasi-static analyses

Fig. 5 presents the system's total base shear-displacement response when subjected to a controlled cyclic displacement history applied at storey #7, whose height, referred to the ground, is $z = 0.7h_w$. The displacement protocol comprises two cycles with increasing amplitudes ranging from 0.1% to 3.5% drift ratio at $z = 0.7h_w$. As the displacement of the plots is measured at the roof level ($z = h_w$), the imposed drifts are not necessarily the same as $DR = \Delta/h_w$. Fig. 5 also presents the hysteresis loops obtained as the sum of the base shear resisted by the four walls analyzed independently. This figure shows how both responses match almost entirely during the whole series of cycles, and are characterized by extensive pinching, but limited unloading stiffness and strength degradation. In addition, Fig. 5 depicts how the monotonic curves of the system, obtained under loading pointing towards the positive direction, matched the backbone curve of the hysteresis loops developing in both directions. The 'negative' monotonic curve is obtained by multiplying the positive counterpart by a factor of (–1), as indicated in the nomenclature of Fig. 5.

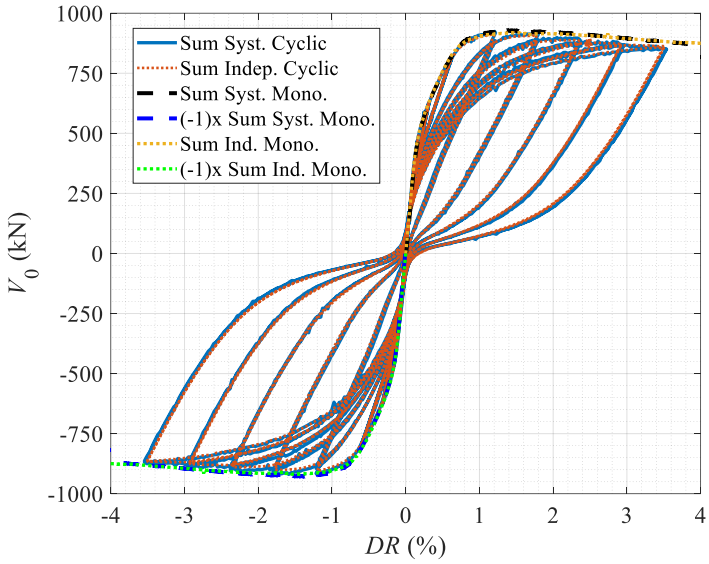

Figure 5. Total V_0-Δ response of the four walls; system and independent cases

Fig. 6 presents the V_0-Δ hysteresis plots of each of the walls, obtained for the system and independent cases. It is clear from this figure that there are significant qualitative differences between the hysteresis loops obtained if the walls are interconnected or not, especially for the two shortest walls. In particular, it is observed that the cyclic response of wall W4 is totally different in both analysis cases, and presents a counterintuitive shape, more similar to a flag-shaped type of hysteresis than to the typical one obtained for RC walls (as that of W2, for instance). Fig. 6 also shows that the shear resisted by the longest wall W1 is smaller for the system than for the independent cases, for example. In addition, Fig. 6 shows that there is a 'non-trivial' response close to the origin of the loops for W3, system case. The yielding displacement of W3, however, seems to follow the same difference pattern than in the monotonic case, as shown in the following.

Fig. 7 presents the hysteresis loops of each of the walls for the system and independent cases separately, and compares them with the positive monotonic curves. Again, the negative monotonic curve is obtained by directly multiplying the positive curve by (-1). Even though the latter may sound trivial, it is not so much. This is because, for the system case, even though the positive monotonic curve is matching the envelope of the cyclic counterpart, the negative is not, for all the walls. This means that, for the system case, it is not the same to carry out the pushover analysis towards the positive and negative directions. The reason behind this finding is the existence of static shear forces in all of the walls, which can be thought of as another consequence of the so-called 'system effect'. For the independent cases, in turn, it is obvious that conducting pushover analyses in the positive and negative directions yields the same results but with opposite sign, because there are no static (sustained) shear forces affecting the walls (left-hand side graphs in Fig. 7). For example, W1 presents a negative permanent base shear force within the system case of -55.5 kN, which renders the negative version of the monotonic curve larger than the backbone curve of the hysteresis loops.

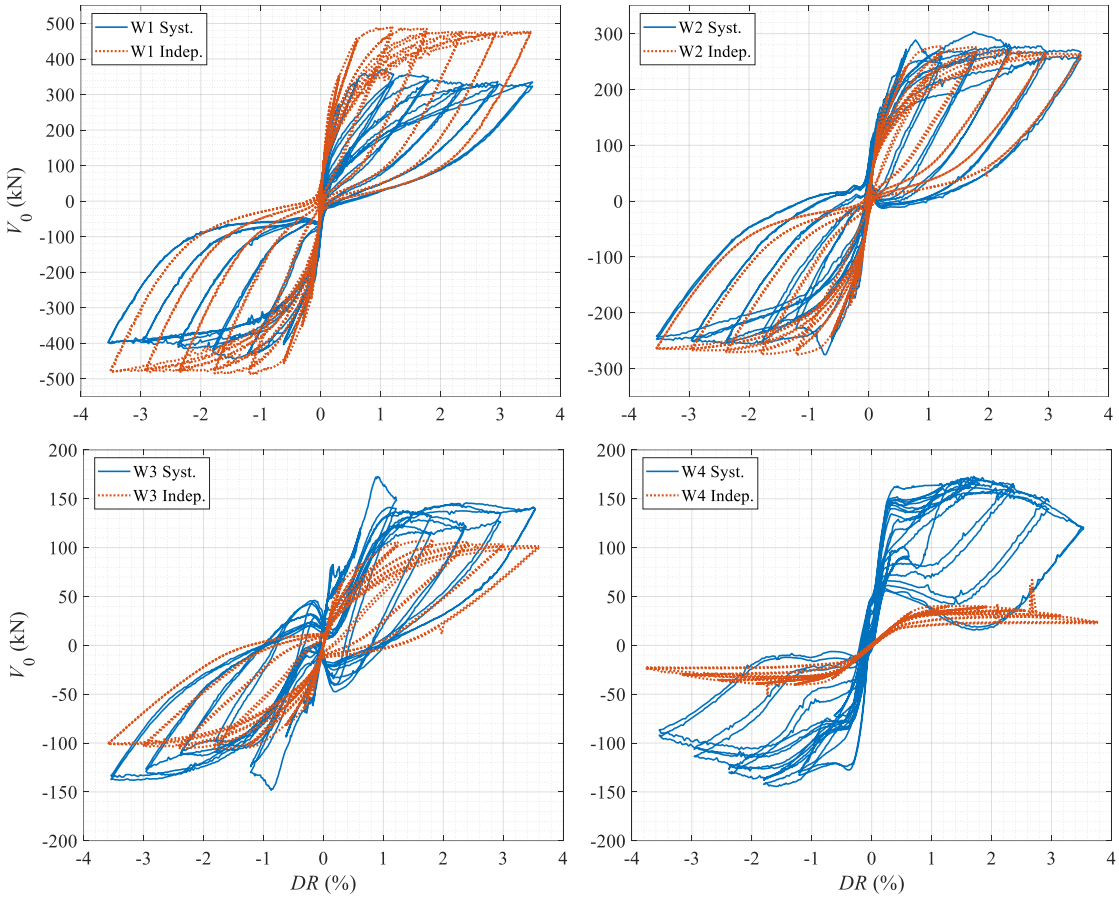

Figure 6. Hysteresis response of walls W1 to W4; system and independent cases

Fig. 8 compares the hysteresis and monotonic curves of the four walls obtained for the system case with the analytical prediction computed with Equations (1) to (3) (α_S = 0.9, 0.65, 0.45, and 0.30, for walls W1 to W4, respectively). The analytical prediction for the negative case is presented in two ways: (1) by simply multiplying the positive curve by (-1), and (2) same as (1), but adding the permanent static base shear ($V_{0,p}$) to the predicted force V_0. The values of $V_{0,p}$ taken by each wall is provided in Fig. 8. Note that the sum of these four permanent shear forces is almost zero. From Fig. 9, it seems clear that the analytical prediction provides a more accurate backbone curve for the cyclic results if it is modified to account for sustained static loads. As noted in Quintana Gallo & Meneses (2021), the existence of a permanent load in the direction of analysis is equivalent to having asymmetrical conditions in the positive/negative yielding conditions of the restoring force, referred to the static equilibrium position. For $V_{0,p} < 0$, both yielding forces increase, whereas for $V_{0,p} > 0$, they decrease (negative yielding is 'more negative'). This explains why if $V_{0,p} < 0$, the derived negative pushover curve underestimates the negative-direction backbone curve of the hysteresis loops, whereas if $V_{0,p} > 0$, they overestimate them.

Of particular interest is the case of W4, which, apparently, is predicted to yield at a smaller *DR* compared to the monotonic case, in both directions. A deeper look into these results, however, shows otherwise, as explained next. Fig. 9 provides a 3-dimensional (3D) representation of the hysteresis loops (Quintana Gallo & Meneses 2021; Quintana Gallo 2023). This figure presents the curve [*DR*, V_0, Step #], which more clearly shows the evolution in 'time' (step #) of the hysteresis loops. With this type of graph, it was possible to spot a very unusual result: the loops of W4 inverted their direction during the initial part of the wall response, where the large shear forces at small *DR* developed. That is to say, some of the cycles developed in the clockwise direction (as usual) but others took place counterclockwise. The graph on the right-hand side of Fig. 9, in turn, shows the 2-dimensional (2D) projection of the left-hand side 3D graph in the *DR*-V_0 plane. It is worth noting that, for reference purposes, the monotonic curves are plotted in the *DR*-V_0 plane of both graphs of Fig. 9. Because there is a step # associated to each of the *DR*-V_0 coordinates of the loops, the direction of evolution of the hysteresis can be directly found. The 3D graph of Fig. 9, which is non-self-intersecting, depicts the direction of the loops. The cyclic results

for W4 predict the development of large shear forces at smaller displacement levels compared to the pushover analyses. Nonetheless, such shear forces are not larger than the maximum achieved at larger drift levels.

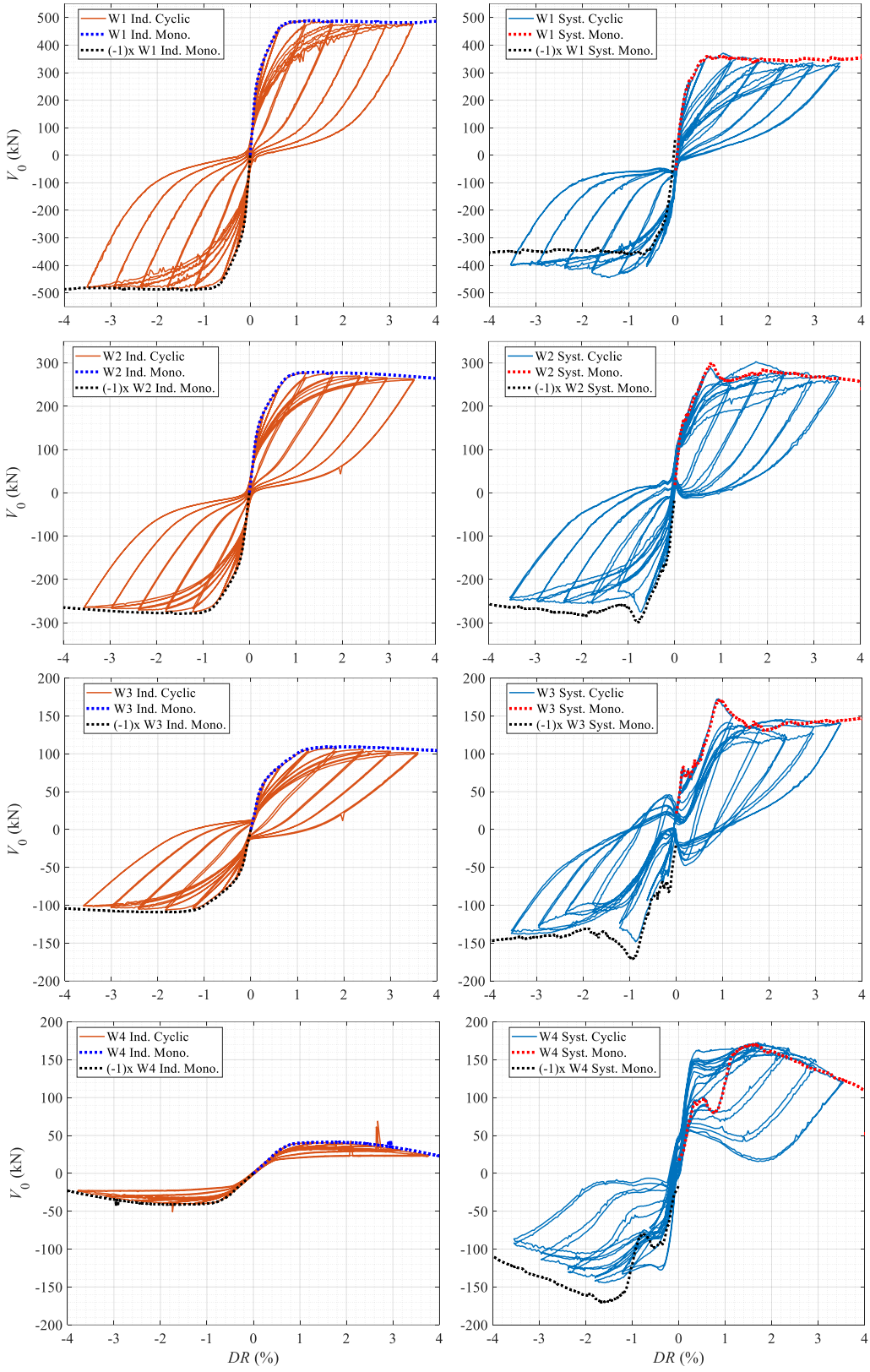

Figure 7. Hysteresis and monotonic responses all walls; system and independent cases

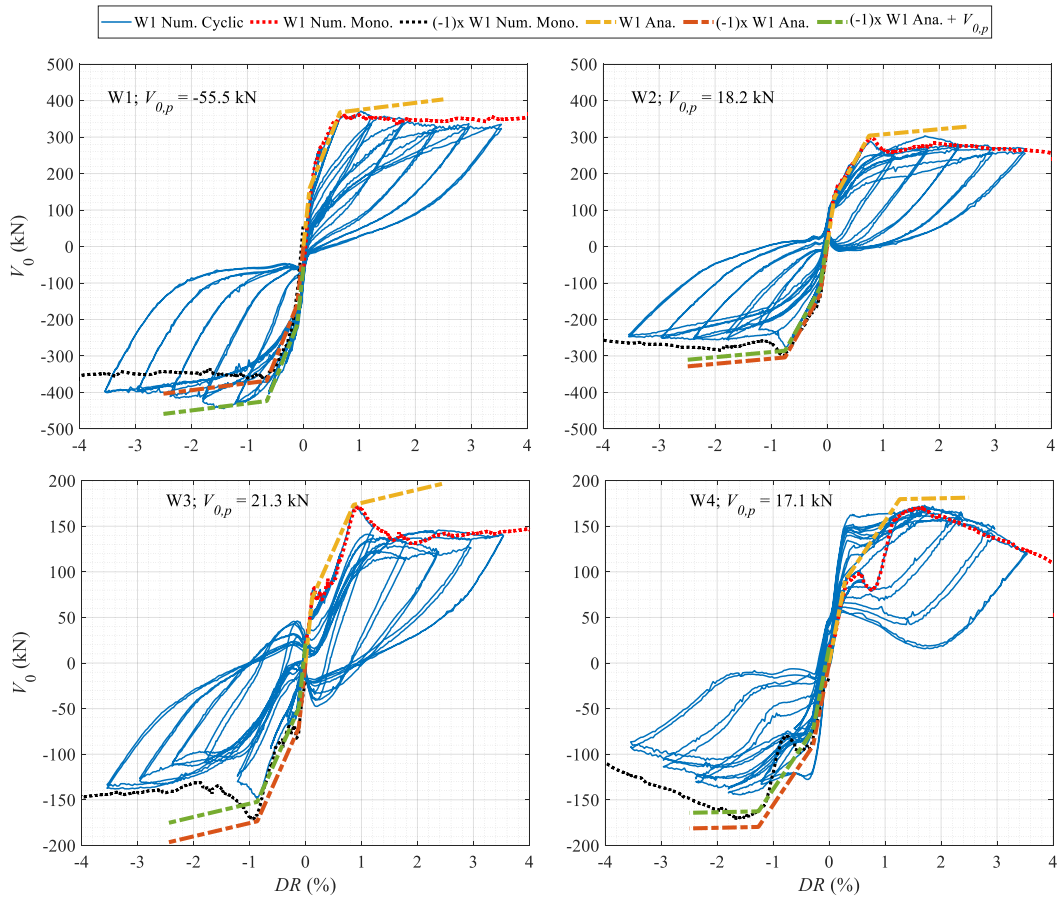

Figure 8. Analytical prediction compared to the cyclic and monotonic responses of all walls, system case

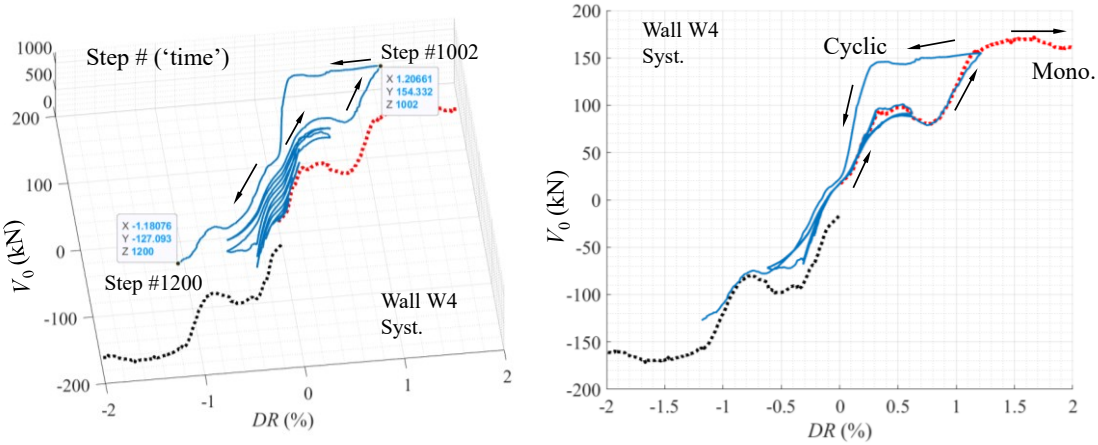

Figure 9. Non-trivial hysteresis of wall W4, system case: 2-dimsensional V_0-DR and 3-dimensional V_0-DR-step# curves

Conclusions

This contribution presented the results of a series of monotonic and cyclic responses of four reinforced concrete (RC) walls part of a case-study building, treated independently and interconnectedly by means of horizontal displacement compatibility at each storey level (rigid diaphragm action). The cyclic analyses showed important differences in the hysteresis response of all the walls under both conditions (system and independent cases). In addition, the paper showed that the monotonic analyses, carried out in previous research do match the envelopes of the cyclic responses, but in the positive direction only, implying differences in the pushover results if the analyses are carried out towards the positive or the negative directions. It was found that

this difference is due to the existence of static permanent base shear forces in all of the walls, which introduce asymmetry into the yielding conditions as the static equilibrium position changes.

The proposed analytical formulation provides conservative and accurate presentations of the monotonic and cyclic envelopes using λ_y = 1.0, except for part of the response of the shortest wall W4, which is predicted to have a very counter-intuitive response with large base shear forces at small drift levels. A deeper look into such a behaviour using 3-dimensional hysteresis plots showed that there is an inversion of the direction of the hysteresis cycles. Such behaviour makes it hard to distinguish at what drift level W4 yields. This could be more clearly found using the plots of the base moment-top displacement plots, which is hopped to be included in an extended version of this work to be published in the future.

It is concluded that the so-called system effect should be somehow considered in the design of RC walls. If it is neglected, the numerical results may not be representative of those predicted within a real building, which in the great majority of the cases would be structured with walls of different lengths. On another relevant note, experimental work on individual walls carried out to date might very likely not be able to replicate what would happen if they were part of a system of several walls, a challenge to the foundations of design specifications. To revise this aspect, experimental work carried out by the authors and collaborators at the time of writing this paper, will be of much use for having the apparently first experimental study on this specific matter to date, able to test the corresponding numerical and analytical predictions. Finally, much more research is needed to find out how this effect can be accounted for if others are also included, such as the coupling introduced by the floor slabs or coupling beams.

Acknowledgements

This paper was written as part of the FB – CTU Global Postdoc Fellowship Program of the Czech Technical University in Prague, Prague, Czech Republic. The support of Prof. František Wald and Dr. Jiří Mareš for writing this contribution is gratefully acknowledged.

References

Álvarez R (2019) Determinación del desplazamiento de fluencia en sistemas de muros de hormigón armado. Memoria de Título, Universidad Técnica Federico Santa María, Valparaíso, Chile (*In Spanish*).

Beyer K, Simonini S, Constantin R, Rutenberg A (2014) Seismic shear distribution among interconnected cantilever walls of different lengths. *Earthq Eng Struct Dyn*, 43:1423‑1441.

Dashti F, Dhakal RP, Pampanin S (2017) Numerical modelling of rectangular reinforced concrete structural walls. *J Struct Eng*, 143(6):04017031

DIANA (2017) Diana user's manual, release 10.1. DIANA FEA BV, Delft, Netherlands.

Paulay T (1983) Deterministic seismic design procedures for reinforced concrete buildings. *Eng Struct*, 5(1):79‑86.

Paulay T, Priestley MJN (1992) Seismic design of reinforced concrete and masonry buildings. Wiley, New York.

Paulay T, Priestley MJN (1993) Stability of ductile structural walls. *ACI Struct J*, 90(4):385‑392.

Quintana Gallo P (2018) Simple estimation of the maximum elastic roof displacement of slender cantilever RC walls accounting for dynamic effects. *Obras y Proyectos*, 23:55‑62.

Quintana Gallo P, Meneses R (2021) On stability of SDOF system with asymmetric hysteresis subjected to seismic excitations. *Int J Struct Stab Dyn*, 21(5):2171002.

Quintana Gallo P, Dashti F, Caballero M, Álvarez R (2022) Shear demand and inelastic displacement capacity of RC walls of different lengths forming a structural system. *Bull Earthq Eng*, 20:7315–7346.

Quintana Gallo P (2023) Novel three-dimensional non-self-intersecting plots for describing the dynamics of structural systems and their hysteresis. EURODYN 2023, Delft, Netherlands.

Rutenberg A (2004) The seismic shear of ductile cantilever wall systems in multistorey structures. *Earthq Eng Struct Dyn*, 33:881‑896.

Wallace JW, Moehle JP (1992) Ductility and detailing requirements of bearing wall buildings. *J Struct Eng*, 118(6):1625-1644.